Research Article

In Situ Investigation of Complex BaSO Fiber Generation in the Presence of Sodium Polyacrylate. 1. Kinetics and Solution Analysis

Tongxin Wang, and Helmut Clfen

Langmuir, **2006**, 22 (21), 8975-8985• DOI: 10.1021/la0609827 • Publication Date (Web): 30 June 2006

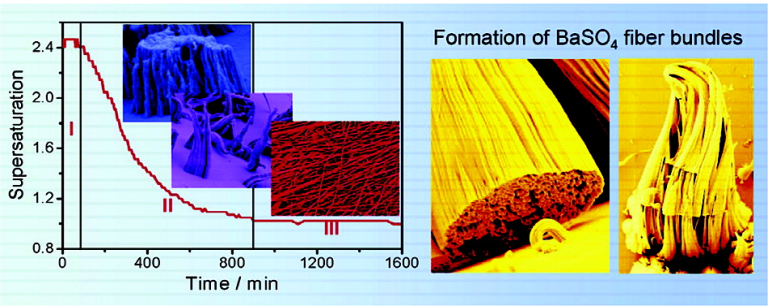

More About This Article

Additional resources and features associated with this article are available within the HTML version:

- Supporting Information
- Links to the 3 articles that cite this article, as of the time of this article download
- Access to high resolution figures
- Links to articles and content related to this article
- Copyright permission to reproduce figures and/or text from this article

View the Full Text HTML

In Situ Investigation of Complex $BaSO_4$ Fiber Generation in the Presence of Sodium Polyacrylate. 1. Kinetics and Solution Analysis

Tongxin Wang† and Helmut Cölfen*

Max-Planck Institute of Colloids and Interfaces, Colloid Chemistry, Research Campus Golm, Am Mühlenberg, D-14424 Potsdam, Germany

Received April 11, 2006. In Final Form: May 26, 2006

Simple solution analysis of the formation mechanism of complex $BaSO_4$ fiber bundles in the presence of polyacrylate sodium salt, via a bioinspired approach, is reported. Titration of the polyacrylate solution with Ba^{2+} revealed complex formation and the optimum ratio of Ba^{2+} to polyacrylate for a slow polymer-controlled mineralization process. This is a much simpler and faster method to determine the appropriate additive/mineral concentration pairs as opposed to more common crystallization experiments in which the additive/mineral concentration is varied. Time-dependent pH measurements were carried out to determine the concentration of solution species from which $BaSO_4$ supersaturation throughout the fiber formation process can be calculated and the second-order kinetics of the Ba^{2+} concentration in solution can be identified. Conductivity measurements, pH measurements, and analytical ultracentrifugation revealed the first formed species to be Ba−polyacrylate complexes. A combination of the solution analysis results and optical microscopic images allows a detailed picture of the complex precipitation and self-organization process, a particle-mediated process involving mesoscopic transformations, to be revealed.

Introduction

Hierarchically organized materials, which are usually formed in solvent phases, have received increased attention in recent years because of their outstanding level of organization and the superior materials properties of biominerals[1,2] as well as increased interest in biomimetic mineralization strategies. (For recent reviews, see refs 3−8.) However, in many if not most cases, the formation mechanism of the complex organic−inorganic hybrid material is unknown. This is an obstacle in obtaining a deeper understanding of the formation of such complex hybrid materials and rational control of the mineralization process. It is difficult to analyze the formation of these materials by a single analytical technique because several length scales usually have to be considered simultaneously. Many microscopic techniques suffer from drying artifacts during sample preparation. These difficulties are frequently encountered in the analysis of biominerals and minerals formed via a bioinspired approach. Therefore, the investigation of complex structure formation processes in solution is a demanding analytical task.

In our previous work, we reported on the formation of interesting $BaSO_4$ and $BaCrO_4$ fiber bundles by polymer-directed crystallization in the presence of double hydrophilic block copolymers (DHBCs)[9−15] or simple polyacrylate.[13,16] More complex structures could be synthesized if a second block copolymer was simultaneously applied.[17] The suggested heterogeneous nucleation mechanism of the fiber bundles[13] was primarily based on electron microscope observations; however, the questions about possible first formed species like complexes still remained. From previous work, it can be concluded that the organic macromolecule in this system is a vital component in the mineralization process because of its involvement in nucleation and growth control. For synthetic analogues of biomolecules, Addadi et al. have investigated the interaction between macromolecules and crystals and have demonstrated that polymers, including their secondary structures, are much more effective in influencing crystal nucleation and growth than the corresponding monomers.[18] Thus, it is important to investigate the first formed species in the complex mineralization process, with special emphasis on the polymer. Herein, we carried out a detailed study on the formation process of the complex hierarchical $BaSO_4$ structures by techniques sensitive to dissolved species and time-dependent optical microscopy in solution. Therefore, we get a detailed picture of the processes taking place in solution, which is complimentary to our extensive microscopic investigations of the same process reported in the second part of this series.[19] This shows that only combined studies of the solution species and the emerging microscopic structures can provide sufficient insight into such complex mineralization processes.

Experimental Section

1. Materials. The following chemicals were purchased from the indicated suppliers and used without purification: Na_2SO_4 (Aldrich,

* Corresponding author. E-mail: coelfen@mpikg.mpg.de. Tel: ++49-331-567-9513. Fax: ++49-331-567-9502.

† Present address: Department of Materials Science and Engineering, University of Pennsylvania, 3231 Walnut Street, Philadelphia, Pennsylvania 19104.

(1) Lowenstam, H. A.; Weiner, S. *On Biomineralization*; Oxford University Press: Oxford, England, 1989.
(2) Mann, S. *Biomineralization − Principles and Concepts in Bioinorganic Materials Chemistry*; Oxford University Press: Oxford, England, 2001.
(3) Mann, S. *Angew. Chem., Int. Ed.* **2000**, *39*, 3392−3406.
(4) Estroff, L. A.; Hamilton, A. D. *Chem. Mater.* **2001**, *13*, 3227−3235.
(5) Cölfen, H.; Mann, S. *Angew. Chem., Int. Ed.* **2003**, *42*, 2350−2365.
(6) Meldrum, F. C. *Int. Mater. Rev.* **2003**, *48*, 187−224.
(7) Yu, S. H.; Cölfen, H. *J. Mater. Chem.* **2004**, 14, 2124−2147.
(8) Cölfen, H. *Curr. Opin. Colloid Interface Sci.* **2003**, *8*, 23−31.
(9) Cölfen, H. *Macromol. Rapid Commun.* **2001**, *22*, 219−252.
(10) Qi, L.; Cölfen, H.; Antonietti, M. *Angew. Chem., Int. Ed.* **2000**, *39*, 604−607.
(11) Qi, L.; Cölfen, H.; Antonietti, M. *Chem. Mater.* **2000,** *12*, 2392−2403.
(12) Yu, S. H.; Cölfen, H.; Antonietti, M. *Chem.—Eur. J.* **2002**, *8*, 2937−2945.
(13) Qi, L.; Cölfen, H.; Antonietti, M.; Li, M.; Hopwood, J. D.; Ashley, A. J.; Mann. S. *Chem.—Eur. J.* **2001**, *7*, 3526−3532.
(14) Yu, S. H.; Cölfen, H.; Antonietti, M. *Chem.—Eur. J.* **2002**, *8*, 2937−2945.
(15) Yu, S. H.; Cölfen, H.; Antonietti, M. *Adv. Mater.* **2003**, *15*, 133−136.
(16) Yu, S. H.; Antonietti, M.; Cölfen, H.; Hartmann, J. *Nano Lett*. **2003**, *3*, 379−382.
(17) Li, M.; Cölfen, H.; Mann, S. *J. Mater. Chem*. **2004**, *14*, 2269−2276.
(18) Addadi, L.; Moradian-Oldak, J.; Weiner, S. *ACS Symp. Ser.* **1991**, *444*, 13−27.
(19) Wang, T.; Reinecke, A.; Cölfen, H. *Langmuir* **2006**, *22*, 8986−8994.

10.1021/la0609827 CCC: $33.50
Published on Web 06/30/2006

99%), $BaCl_2$ (Aldrich, 99%), and polyacrylate sodium salt (PAANa, $M_n = 5100$ g·mol^{-1}) (Fluka). The sodium content of the polymer was reported by the manufacturer to be 19% w/w, implying that only a minority of the carboxylic groups were protonated.

2. $BaSO_4$ Mineralization. An aqueous solution of 0.6 mL of 0.05 mol·L^{-1} $BaCl_2$ was added dropwise to 15 mL of PAANa (0.56 g·L^{-1}) in a glass bottle under vigorous stirring. Then, 0.6 mL of 0.05 mol·L^{-1} Na_2SO_4 was added dropwise and was stirred for 5 min. Solution pH was adjusted to 5.6 to 5.7 using HCl. Then, the solution was transferred into glass or polypropylene bottles and kept standing quiescent for a defined period for mineralization at room temperature.

3. Analytical Techniques. *Optical Microscopy.* Optical microscopy images were taken in solution with an Olympus BX41 microscope equipped with a Monacor TVCCD-460 color camera. Time-resolved optical microscopy (TROM) was measured by phase-contrast microscopy as described elsewhere.[20] Briefly, a temperature-controlled (20 °C) observation chamber composed of a glass substrate was filled with solution, tightly sealed, and inspected under a phase-contrast microscope (Zeiss 35, 40, Ph 2). The structures are oriented mainly along the glass substrate but show fluctuation out of the focal plane of the microscope. Suitable defined areas were selected, and a TROM video on this selected area was taken over 48 h. Parts of this video can be seen in the Supporting Information to ref 19.

Conductivity and pH Measurements. Conductivity measurements were performed in a glass bottle under vigorous stirring with a CDM 92 conductivity meter (Radiometer Copenhagen) connected to a BETA Sensor conductivity cell (C-100-8-T, Sweden). pH measurements were completed with a 716 DMS Titrino pH meter (Metrohm), simultaneously with the conductivity measurement. Time-resolved pH measurements for the mineralization solution were made automatically in a glass bottle over 66 h by a 702 SM Titrino pH meter (Metrohm) connected to a computer with Tinet version 2.4 software under quiescent conditions. The pH readings were taken with an accuracy of 0.01 pH unit.

Determination of Appropriate Concentrations of Ba^{2+} in the Presence of Different Concentrations of PAANa. Generally, these measurements were carried out on a series of concentrations of PAANa solution from 0.035 to 5.6 g/L. First, the titration of Ba^{2+} solution into a defined concentration of PAANa solution (18 mL) and the titration line of a volume of Ba^{2+} solution versus the corresponding variation in pH were recorded simultaneously. After fitting the plot to a linear equation, point A can be read from the point that first deviates from the straight line to the curved part. Then, a series of concentrations of Ba^{2+} can be read from a series of point As. The curve of the concentrations of Ba^{2+} versus the corresponding concentration of PAANa is the appropriate concentration pair of Ba^{2+} and the corresponding PAANa.

Analytical Ultracentrifugation. Analytical ultracentrifugation was performed with an Optima XL-I (Beckman Coulter, Palo Alto, CA) in self-made 12 mm double-sector titanium center pieces at 25 °C and 60 000 rpm applying Rayleigh interference optics. The cells were filled with 320 μL of solution and water as a reference. To make the sample signal detectable, the concentrations of Ba^{2+} and polyacrylate sodium for analytical ultracentrifugation are 0.02 mol/L and 6 g/L or 0.2 mol/L and 60 g/L, respectively, which are higher than the solution pairs in our mineralization experiments by a factor of 10 or 100. The sedimentation coefficient distributions were evaluated using the program SEDFIT by Schuck.[21]

Results and Discussion

Complexation between Ba^{2+} Ions and $RCOO^-$ Groups. The first question pertaining to the growth mechanism of the complex fibrous $BaSO_4$ superstructures, in the presence of polyacrylate, concerns the first formed species after the addition of Ba^{2+} and SO_4^{2-} to a sodium polyacrylate solution. Previous studies indicate that Ba^{2+} binds strongly to carboxylate groups.[13] Here we applied analytical ultracentrifugation (AUC) to reveal the sedimentation coefficient distribution, which is proportional to the polymer molar mass distribution and the polymer density, to check for Ba^{2+}−polymer complexes (Figure 1).

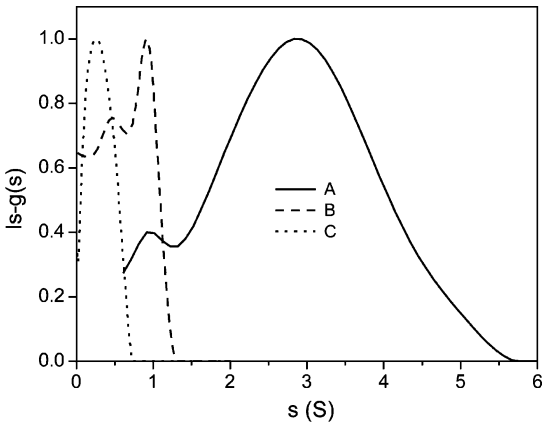

Figure 1. Differential sedimentation coefficient distribution ls-g(s) of polyacrylate and before and after addition of Ba^{2+} without correction for diffusion broadening. (A) $[Ba^{2+}] = 0.2$ mol/L, [PAANa] = 60 g/L; (B) $[Ba^{2+}] = 0.02$ mol/L, [PAANa] = 6 g/L; (C) $[Ba^{2+}] = 0$, [PAANa] = 6 g/L.

It is obvious that the sedimentation coefficient distribution (s distribution) shifts to higher sedimentation coefficients, indicating a molar mass and/or density increase due to the formation of a Ba^{2+}−polymer complex when Ba^{2+} is added to polyacrylate. At a low Ba^{2+} concentration of 20 mM (B in Figure 1), the s distribution is bimodal, where one peak is attributed to polyacrylate with complexed Ba^{2+} and the other is attributed to several polymer chains. At a higher Ba^{2+} concentration, the s distribution shifts to higher sedimentation coefficients and becomes further broadened, indicating the aggregation of polyacrylate by complexation with Ba^{2+} and a density increase of the polymer (A in Figure 1). It is interesting that the 10-fold increase in the concentrations of both Ba^{2+} and polymer from B to A in Figure 1 yields different complexes, indicating a nonstoichiometric and kinetically driven complex-formation process rather than a thermodynamically driven one, where similar trends are expected for the given reactant concentration ratio. The above results clearly show the complexation of Ba^{2+} ions with the $RCOO^-$ groups in PAA molecules and are in agreement with a literature report revealing Ca^{2+} coordination to polyacrylate.[22]

To gain more quantitative insight into $Ba^{2+}/RCOO^-$ complex formation, pH variation upon titration of the polyacrylate sodium solution with NaCl or $BaCl_2$, respectively, was investigated at the same original pH and ionic strength (Figure 2).

The raw data from NaCl and $BaCl_2$ in Figure 2a show very different behaviors. The addition of $BaCl_2$ solution to the PAANa solution shows a much more pronounced pH decrease due to proton release upon Ba^{2+} coordination to the poly(acrylic acid), which reveals a strong complexation between Ba^{2+} and $RCOO^-$ in PAA (eqs 1 and 2). The addition of NaCl at the same original pH and ionic strength shows only a slight linear pH decrease, which can be attributed to the diverse salt effect of NaCl. The presence of diverse salt (not containing ions common to the equilibrium involved) will cause an increase in the dissociation of a weak acid (e.g., PAA).[23] The PAANa used here has a rather high sodium content (19% w/w), which means that only a small percentage of the carboxylate groups were protonated (∼12.9% molar ratio of carboxylate groups, see the Appendix for the

(20) Reinecke A.; Döbereiner, H. G. *Langmuir* **2003,** *19,* 605−608.
(21) Schuck P. *Biophys. J.* **2000**, *78*, 1606.
(22) Sinn, C. G.; Dimova, R.; Antonietti, M. *Macromolecules* **2004**, *37*, 3444−3450
(23) Christian, G. D. *Analytical Chemistry*; John Wiley & Sons: New York, 1986.

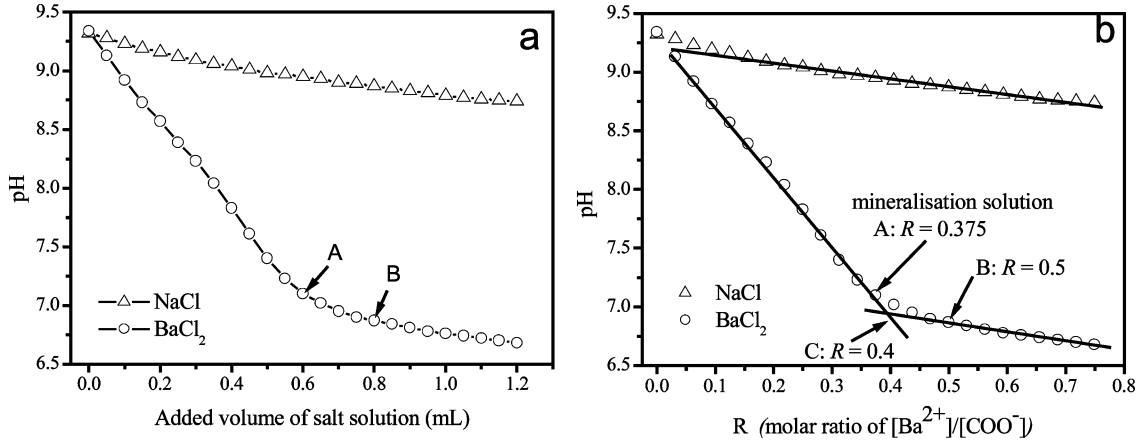

Figure 2. pH variation of PAANa (15 mL, 0.56 g/L, pH 9.3) solution upon titration with $BaCl_2$ (0.05 mol/L, pH 6.89) or NaCl (0.1 mol/L, pH 6.88). (a) pH variance with the added volume of $BaCl_2$ solution; (b) pH variance with the molar ratio of total Ba^{2+} ions to total carboxylate groups in solution. ($R = [Ba^{2+}]_{total}/[COO^-]_{total}$; for the case of NaCl, $R = {}^1/_2\{[Na^+]_{total}/[COO^-]_{total}\}$). Point A is the experimental concentration of Ba^{2+} (~1.92 mmol/L) in the presence of 0.56 g/L PAANa, which was generally used in the previous mineralization experiments.[13,16] Point B is the theoretical point where all COO^- groups are "saturated" by the added Ba^{2+}. (See the calculation in the Appendix.)

detailed calculation.) In this case, resulting from the acid-dissociation equilibrium constant (K_a) of the equilibrium between $RCOO^-$ and RCOOH in PAANa solution, part of the $RCOO^-$ will be protonated and consume some protons so that the original solution becomes slightly basic (pH ~9) (eq 1).

With the addition of Ba^{2+}, the pH will decrease because of the shift of eq 1 to the product side, which in turn results from a product-side shift of eq 2 due to the complexation of Ba^{2+} with $RCOO^-$ in the PAANa solution.

$$RCOOH + H_2O \overset{K_a}{\rightleftharpoons} RCOO^- + H_3O^+ \quad (1)$$

$$2RCOO^- + Ba^{2+} \overset{K_c}{\rightleftharpoons} (RCOO)_2Ba \quad (2)$$

$$BaSO_4 \overset{K_{sp}}{\rightleftharpoons} SO_4^{2-} + Ba^{2+} \quad (3)$$

The situation becomes clearer in Figure 2b where the amount of added salt is normalized by the molar ratio of ions. (The molar ratio is defined as $R = [Ba^{2+}]_{total}/[COO^-]_{total}$ or $R = {}^1/_2\{[Na^+]_{total}/[COO^-]_{total}\}$ for the case of NaCl.) Clearly, there are two linear parts in the $BaCl_2$ graph with greatly different slopes and a transition point around a molar ratio of $R = 0.4$. There are three important points in Figure 2: points A−C, where the R ratios are 0.375, 0.4, and 0.5, respectively.

When the added amount of Ba^{2+} is lower than point A, the addition of Ba^{2+} leads to a pronounced decrease in the solution pH, indicating complex formation between PAA and Ba^{2+} according to eq 2. The decreasing in detected pH implies that the formation of the complex will lead to a right shift of the acid dissociation of PAA in eq 1. The curved part with a decreased slope after point A shows that full saturation of the carboxylate groups by Ba^{2+} is not achieved. Point A in Figure 2 marks the point of the first deviation from the full complexation of Ba^{2+} with the carboxylate groups. This is a meaningful experimental concentration for slow mineralization because the supersaturation can be kept low by ion complexation. Between points A and B, the line is curved instead of straight, which means that additional Ba^{2+} weakly influences the acid dissociation and at least some excess Ba^{2+} ions can no longer be complexed by carboxylate groups. Therefore, it is easily understood that the concentration at point A was generally used for $BaSO_4$ fiber generation in the presence of PAA (Figure 2).[13,16]

At a molar ratio of R greater than 0.5 (point B), the slope for $BaCl_2$ is identical to that for NaCl, indicating that no more protons are released from the polyacrylate upon addition of Ba^{2+}. This implies that most of the carboxylate groups in PAA(Na) are complexed by Ba^{2+} and that the addition of more Ba^{2+} has no further influence on the acid dissociation/association of PAA.

Point B is the concentration where all of the $RCOO^-$ groups are complexed completely by the added Ba^{2+} ($R = 0.5$), which is an indication that each Ba^{2+} combines with two $RCOO^-$ groups. After that, there will be no additional carboxylate groups that can be complexed with the additional Ba^{2+} because the $RCOO^-$ ions were "saturated" by the Ba^{2+}. Therefore, the addition of more Ba^{2+} will result in free Ba^{2+} instead of the complex. Consequently, a slow mineralization speed, resulting from the necessary dissociation of Ba^{2+} from the polymer complex, cannot be reached at this point because of the higher free Ba^{2+} concentration in solution.

The above results indicate that the concentration of free and complexed Ba^{2+} by PAA can be indirectly accessed by a simple pH measurement. For different PAA concentrations, the titration plot has the same characteristic decrease in slope upon full complexation of Ba^{2+} by carboxylate.

Further evidence of Ba^{2+} complexation by polyacrylate can be obtained from conductivity measurements (Figure 3b). It is shown that there is also a change in the slope of the curves at A_1 and A_2 in Figure 3b, which are at exactly the same Ba^{2+} concentrations as for A_1 and A_2 in the pH plots shown in Figure 3a. The smaller increase in the conductivity below A_1 and A_2 in Figure 3b means that most of the added Ba^{2+} is complexed by PAANa and therefore does not contribute to the conductivity very much, whereas the higher slopes above points A_1 and A_2 in Figure 3b indicate the presence of free Ba^{2+} after saturation of the carboxylate groups by complexed Ba^{2+}. The agreement between Figures 3a and 3b proves that it is possible to determine the appropriate concentration of Ba^{2+} for the saturation of PAANa by conductivity and pH titration, where the appropriate concentration of Ba^{2+}, with respect to PAANa, should be around point A. Therefore, an effective Ba^{2+} concentration for slow $BaSO_4$ crystallization experiments can be determined for a given PAA concentration (Figure 3a and c). Generally, from the first point of deviation from the steep slope (A), the appropriate concentration ratio of Ba^{2+} versus PAANa can be determined.

On the basis of pH variation upon titration of Ba^{2+} into a series of PAANa at different initial concentrations (Figure 3c),

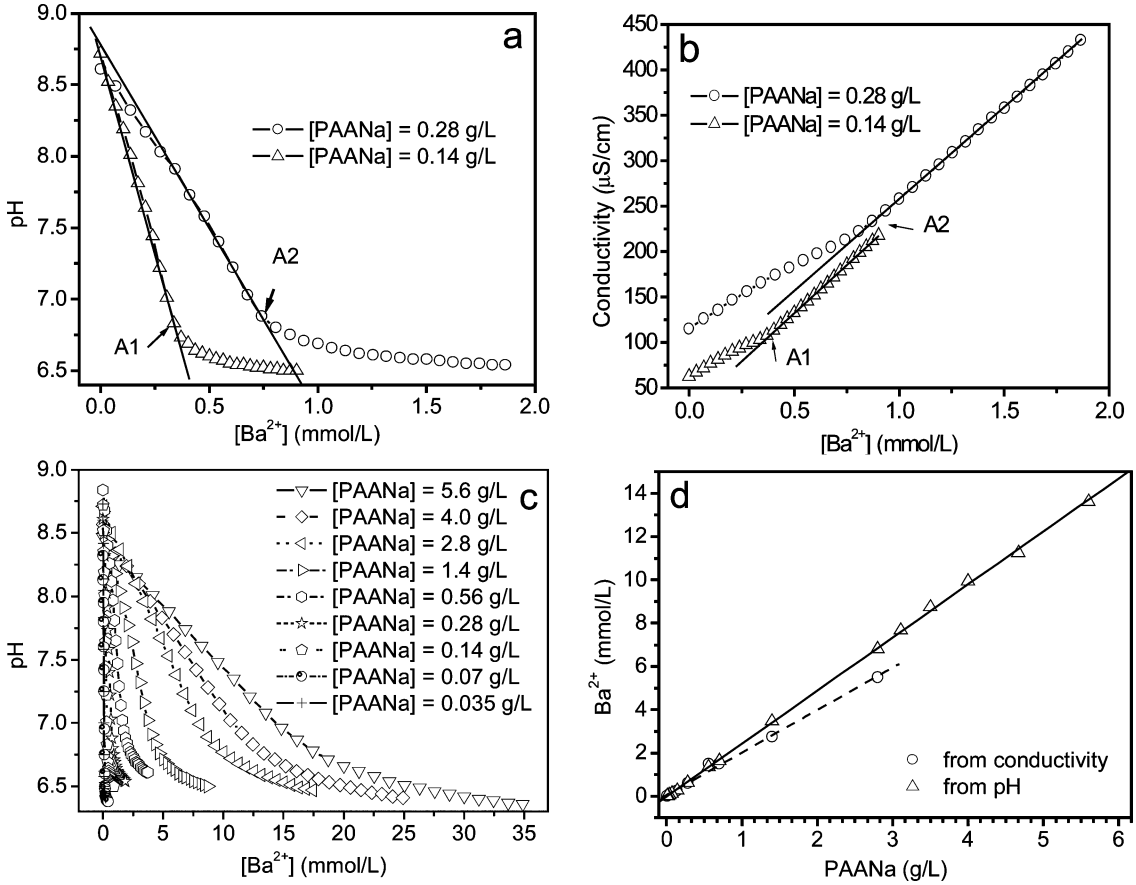

Figure 3. (a) pH variation of PAANa solution upon titration with $BaCl_2$. (b) Typical conductivity variation in the same experiment as in part a. (c) Series of pH variations of different concentrations of PAANa (18 mL) solution upon titration with $BaCl_2$. (d) Appropriate mineralization concentration of Ba^{2+} in the presence of different concentrations of PAANa obtained from pH and conductivity detection. The data are fitted by a line through the origin.

a series of appropriate concentrations of Ba^{2+} in the presence of different concentrations of PAANa can be determined (Figure 3d). Generally, for a series of given concentrations of PAANa solutions, a plot of the titration volume of Ba^{2+} solution versus the corresponding pH was recorded simultaneously, as seen in Figure 3a and c. After fitting the plot to a linear equation, point A can be read at the point that first deviates from the straight line to the curved part. Figure 3d is a plot of the concentration of Ba^{2+} versus the concentration of PAANa. The plot of the concentration of Ba^{2+} (from point A) versus the corresponding concentration of PAANa is the appropriate concentration pair of Ba^{2+} and the corresponding PAANa (Figure 3d).

Similarly, the corresponding plot from conductivity can be also drawn, and the results from pH and conductivity measurements agree reasonably well (Figure 3d). The possible correlation of the saturation points of carboxylate complexation by Ba^{2+} for different PAANa concentrations allows one to use Figure 3d to determine the Ba^{2+} concentration for a given PAANa concentration in order to achieve slow mineralization and slow $BaSO_4$ fiber growth. Therefore, it is now possible to state suitable experimental conditions for a given PAANa concentration to obtain $BaSO_4$ fibers.

Interestingly, the plots of pH and conductivity in Figure 3d are almost linear. By fitting the two plots in Figure 3d with linear equations, slopes of 2.46 and 1.97 can be obtained from pH and conductivity plots, respectively. The slope is equal to the ratio, R, where $R = [Ba^{2+}$ (in mmol/L)]/[PAANa (in g/L)]. From the slope, any concentration of $[Ba^{2+}]$ can be easily obtained if a definite concentration of PAANa is selected.

The pH measurement is a simple method of determining the appropriate concentration over a wide concentration range of PAANa. However, in our case, the mineralization concentration can also be calculated on the basis of the unit number of functional groups in solution because the polymer structure is precisely known. (See the Appendix for detailed calculations.) The transfer of this methodology to more complicated crystallization additives with unknown structure, such as biopolymers extracted from biominerals, should also be possible. This could help to elucidate the interaction between inorganic ions and the organic additive[24−26] and to determine the effective additive concentration for slow mineralization. This is much simpler than other experimental methods such as common crystallization experiments in which the concentration of the additive is varied.[13,27−31] In addition, these results suggest that simple pH monitoring is an effective method of monitoring polymer-controlled mineralization processes as long as the mineralization itself is pH-independent.

Competition of PAANa and SO_4^{2-} for Ba^{2+} and Precipitation of $BaSO_4$ in the Presence of PAANa. The above findings show that for the applied mineralization conditions of $BaSO_4$, Ba^{2+} is complexed by the carboxylate groups of PAANa and the Ba−PAA complex is the first formed species in the formation of complex fiber bundles. It is of interest to investigate what happens upon the addition of sulfate ions. The corresponding experimental results are shown in Figure 4. The addition of NaCl to a PAANa solution leads to a slight pH drop and a conductivity increase. This trend is continued steadily after the addition of sulfate (curves A1 and A2 in Figure 4a and b).

However, the addition of Ba^{2+} to PAANa leads to the pronounced pH decrease already discussed above, but the addition

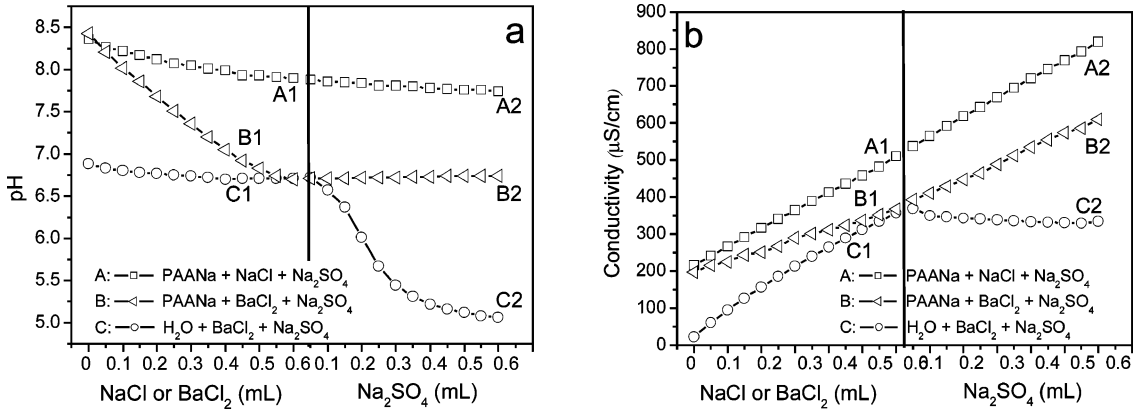

Figure 4. (a) pH variation and (b) conductivity variation of the titration of NaCl (0.1 mol/L, pH 5.0) into 15 mL of PAANa (0.56 g/L) (plot A), $BaCl_2$ (0.05 mol/L, pH 5.0) into 15 mL of PAANa (0.56 g/L) (plot B), and $BaCl_2$ (0.05 mol/L, pH 5.0) into 15 mL of water (plot C). After the point indicated by the vertical line, the given volume of Na_2SO_4 (0.05 mol/L) was added to solutions A−C.

of sulfate, interestingly, leads to a constant pH with increasing sulfate content. Accordingly, a change in the slope of the conductivity versus added ion concentration curve leads to a similar but slightly less steep slope than that observed in the PAANa + NaCl case (curves B1 and B2 in Figure 4a and b). This means that the vast majority of sulfate remains as free ions in solution and does not directly form $BaSO_4$ because it has to compete with the PAA carboxylate groups for Ba^{2+}, which prevents immediate crystallization. The control experiment without PAANa leads to the expected result of immediate $BaSO_4$ nucleation, as evident from a decrease in pH[32] and an immediate change in the conductivity versus ion concentration curve (curves C1 and C2 in Figure 4a and b). The nonincreasing conductivity with increasing sulfate concentration indicates that all added sulfate is directly consumed for $BaSO_4$ formation. The high background conductivity is caused by the Na^+ and Cl^- counterions.

These results show that the stability of the Ba−PAANa complex must be rather high, as can be expected from the low solubility of $BaCO_3$ ($K_{sp}(BaCO_3) = 2.58 \times 10^{-9}$ mol^2/L^2), although the solubility of $BaSO_4$ is lower ($K_{sp}(BaSO_4) = 1.07 \times 10^{-10}$ mol^2/L^2). Therefore, Ba^{2+} should be released from the Ba−PAANa complex upon sulfate addition. However, $BaSO_4$ nucleation is considerably slowed by Ba^{2+} complexation (Figure 4), and polymer interactions with the growing crystal become likely.

In addition, the ionic growth mechanism for $BaSO_4$, in which crystals are grown by direct precipitation of simple Ba^{2+} and SO_4^{2-} ions, will be inhibited. This results from the strong Ba^{2+} complexation by PAANa. Instead, the complex should serve as the precursor for the mineralization, shifting the mechanism from classical ion-mediated crystallization to mesoscale assembly.[5] This is supported by some simple calculations: For the commonly applied total Ba^{2+} and SO_4^{2-} concentrations (1.85 mmol/L), we obtain a supersaturation of 179 in the absence of PAANa because $K_{sp}(BaSO_4) = 1.07 \times 10^{-10}$ mol^2/L^2. However, in the presence of 5.35 mmol/L total COO^- concentration in the PAA solution, almost all of the Ba^{2+} should be complexed by COO^-, resulting in a very low supersaturation.

Crystallization Kinetics. From the above results, it becomes clear that the first species formed in solution is a barium−polyacrylate complex and that the barium-enriched environment serves as a nucleation center for $BaSO_4$ upon sulfate addition because $BaSO_4$ is a sparingly soluble salt. Nevertheless, the release of Ba^{2+} ions from the polyacrylate complex upon crystallization is hindered by the strong Ba^{2+} complexation and results in a pH increase during mineralization (Figure 5a).

On basis of the relevant equilibria shown in eqs 1−3, we were able to calculate the $BaSO_4$ supersaturation via simple pH measurements. The time-dependent supersaturation is calculated according to the procedure, which is shown in detail in the Appendix. On the basis of the time-resolved pH measurements, [Ba^{2+}] in solution can be calculated from a combination of eqs 1 and 2. Assuming that the supersaturation is 1 at a rather long time close to system equilibration (e.g., all $BaSO_4$ has precipitated; in our case, we took the supersaturation at the end of the mineralization reaction to be 1), the supersaturation at different times can be calculated. Moreover, the total [Ba^{2+}] released from the Ba^{2+} complex with carboxylate groups can also be calculated. (See the Appendix for the detailed calculation procedure.)

Because most Ba^{2+} was complexed by PAANa, as evidenced by pH or conductivity titration and AUC measurement, free Ba^{2+} was kept at a rather low concentration ($\sim 10^{-7}$ mol/L, Figure 5c). Hence, even though the SO_4^{2-} concentration is high (around 1.85 mmol/L because no complex formation takes place), the low free [Ba^{2+}] maintains a low supersaturation (Figure 5b), which is necessary for the mineralization process.

Time-dependent pH measurements (Figure 5a) indicate that Ba^{2+} and carboxylate were only slowly released from the complex with time, according to the expectation that Ba^{2+} is complexed strongly by the polyacrylate. In stage I, there is an induction period where no pH change is monitored (0−90 min). This indicates that polyacrylate acts as a crystallization inhibitor for $BaSO_4$ and strongly suggests that the nucleation of the first nuclei begins within the Ba-enriched polymer complexes because the $BaSO_4$ supersaturation is highest in this period and should be

(24) Addadi, L.; Weiner, S. *Proc. Natl. Acad. Sci. U.S.A.* **1985**, *82*, 4110−4113
(25) Aizenberg, J.; Hanson, J.; Koetzle, T. F.; Weiner, S.; Addadi, L. *J. Am. Chem. Soc.* **1997**, *119*, 881−886.
(26) Berman, A.; Addadi, L.; Weiner, S. *Nature* **1988**, *331*, 546−548.
(27) Rudloff, J., Cölfen, H., *Langmuir* **2004,** 20, 991−996.
(28) Cölfen, H.; Qi, L. M. *Chem.−Eur. J.* **2001**, *7*, 106−116.
(29) Shi, H. T.; Wang, X. H.; Zhao, N. N.; Qi, L. M.; Ma, J. M. *J. Phys. Chem. B* **2006**, *110*, 748−753.
(30) Shi, H. T.; Qi, L. M.; Ma, J. M.; Cheng, H. M. *J. Am. Chem. Soc*. **2003**, *125*, 3450−3451.
(31) Luo, L. B.; Yu, S. H.; Qian, H. S.; Gong, J. Y. *Chem. Commun*. **2006**, *7*, 793−795.
(32) Because of the existing equilibria in solution:

$$HSO_4^- \rightleftharpoons SO_4^{2-} + H^+ \qquad pK_a = 1.99$$

$$Ba^{2+} + SO_4^{2-} \rightleftharpoons BaSO_4\downarrow \qquad K_{sp}(BaSO_4) = 1.07 \times 10^{-10}\ \text{mol}^2\ \text{L}^2$$

After mixing a solution of $BaCl_2$ and Na_2SO_4, the solution pH will decrease because of the right shift of the following equilibrium:

$$Ba^{2+} + HSO_4^- \rightleftharpoons BaSO_4\downarrow + H^+$$

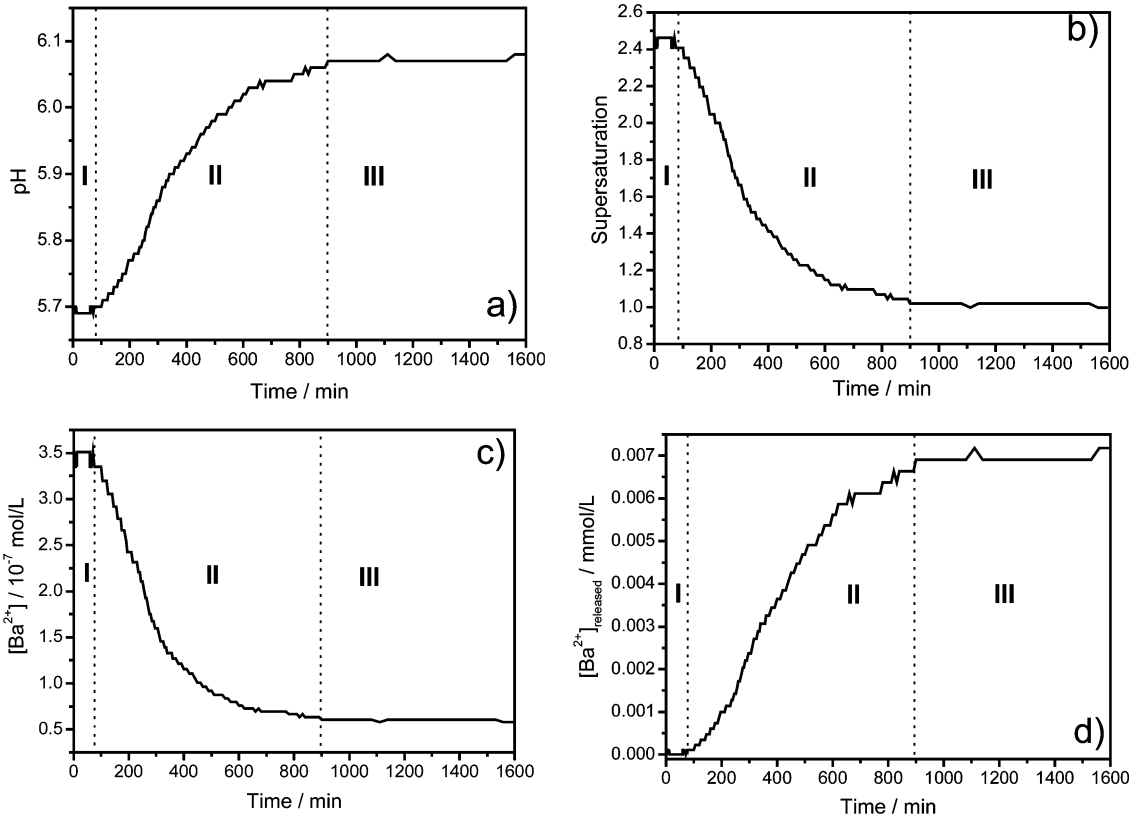

Figure 5. Time-dependent measurement during $BaSO_4$ crystallization from the mixture of $BaCl_2$ (1.92 mmol/L) and Na_2SO_4 (1.92 mmol/L) in the presence of 0.56 g/L PAANa. Note the different zones: I = crystallization inhibition, II = crystallization and III = equilibration. (a) pH; (b) supersaturation of the mixture; (c) concentration of free Ba^{2+} in solution; and (d) total Ba^{2+} concentration released from the complex of Ba^{2+} with carboxylate groups of PAANa vs mineralization time.

sufficient to result in $BaSO_4$ crystallization. Even though the total concentration of released Ba^{2+} was increasing steadily with time (Figure 5d), a rather low concentration of free Ba^{2+}, resulting in low supersaturation, was kept during the whole period (Figure 5b). This is a crucial factor in obtaining a slow crystallization speed.

After the initial induction period I, we observe a sigmoidal pH increase up to 900 min (Figure 5a), coupled with an inverse supersaturation decrease down to 1.02 (Figure 5b) and a sharp decrease in the Ba^{2+} concentration in solution (Figure 5c). All of these observations indicate that most nucleation and particle growth processes take place within period II. At times greater than 900 min, the pH and supersaturation remain almost constant, and the supersaturation drops from 1.02 to 1. This indicates that the nucleation and growth processes have ended and that further structure development of the $BaSO_4$ hybrid particles can take place only via mesoscale transformation of preformed precursor particles, which is indifferent to supersaturation.[5]

Kinetic fitting for the above plot of the free Ba^{2+} concentration versus time can provide further information about the growth kinetics. As an example, the time dependence of the free $[Ba^{2+}]$ concentration in solution (Figure 5c) was fitted by zeroth-, first-, or second-order reaction rate laws. For times before 90 min (inhibition period) or after 900 min (end of the crystallization reaction), no meaningful dependence can be obtained for any reaction kinetics because of the slow reaction times before 90 min or after 900 min. Essentially, a linear dependence was found only for times between 230 and 660 min, indicative of second-order kinetics. Figure 6a is the corresponding plot of $1/[Ba^{2+}]$ versus time with a second-order kinetics fit line of the time-dependent free $[Ba^{2+}]$ from 230 to 660 min. The reaction constant is ca. $k = (2.35 \pm 0.02) \times 10^4$ L mol^{-1} min^{-1}.

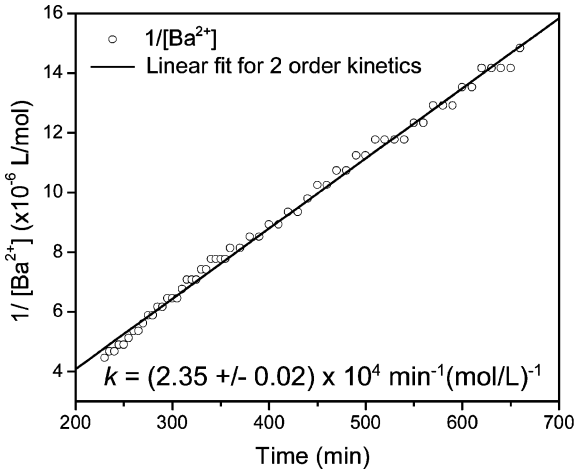

Figure 6. Second-order kinetics fitting of the time-dependent free Ba^{2+} concentration in solution. (See also Figure 5c.) Plot of $1/[Ba^{2+}]$ versus time from 230 to 660 min during $BaSO_4$ crystallization from the mixture of $BaCl_2$ (1.92 mmol/L) and Na_2SO_4 (1.92 mmol/L) in the presence of 0.56 g/L of PAANa.

It is reasonable that the reaction shows second-order kinetics in the regime of nucleation and growth. The reaction velocity depends on the concentration of two species because the free $[Ba^{2+}]$ in solution is generated via two reaction routes: release from the $(RCOO)_2Ba$ complex, which is the complex between PAANa and Ba^{2+}, and dissolution of $BaSO_4$, as shown in eqs 2 and 3. Reaction 4 is the typical second-order reaction A + B → C.

$$[Ba^{2+}_{(eq\ 2)}] + [Ba^{2+}_{(eq\ 3)}] \rightarrow [Ba^{2+}_{free}] \qquad (4)$$

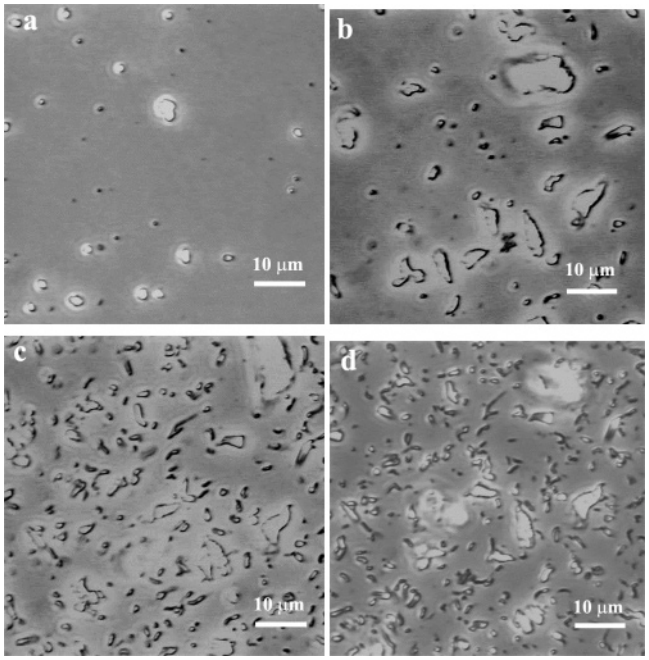

Figure 7. Typical images of time-dependent optical microscopy from the same observed area at different crystallization times: (a) 60 min; (b) 210 min; (c) 12 h; and (d) 24 h. The sample was examined in solution at a constant temperature of 20 °C, and an identical observation area is shown for all images. The full video sequence is shown in Supporting Information.

Consequently, the generation of Ba^{2+} was slow during times of 90−230 (crystallization inhibition) and 660−900 min (end of crystallization). Between 230 and 660 min, the higher rate of Ba^{2+} generation in solution confirms that most nucleation and particle growth processes take place during this period.

To correlate the physicochemical kinetic characterization of the mineralization process in Figure 5 to visual information about the formed $BaSO_4$ crystals and their superstructures, we applied time-resolved optical microscopy (TROM). TROM was performed in the same observation area for 48 h.

The time-resolved TROM study reveals that motionless particles are within the micrometer range. These are aggregates of amorphous $BaSO_4$ nanoparticles, as determined by TEM, and selected-area electron diffraction[19] in the first 60 min (Figure 7a) besides fast-moving nanoparticles. Although the time-resolved pH measurements and their derivative supersaturation and released Ba^{2+} curves (Figure 5) clearly indicate nucleation inhibition, the microscopy images show nucleated nano- as well as microparticles. This is reasonable because the supersaturation is maximum at this time (Figure 5b). Nevertheless, a supersaturation of 2.4 is still low and the small number of nucleated particles does not change the supersaturation to a significant extent in the first 60 min, so this period is generally characterized by nucleation inhibition. There is no significant particle growth within this period.[19] Most of the particles are amorphous nanoparticles or aggregates thereof.[19] Between 90 and 900 min (zone II in Figure 5), a large number of additional particles have nucleated and grown, and the first fiber bundle structures start to develop (Figure 7b and c). It has to be noted that the number of moving particles has also significantly increased.[19] This is expected in the nucleation period between 90 and 900 min. However, the formation of the first fiber bundles indicates that in the present case we are not dealing with the classical nucleation burst following a critical supersaturation according to the LaMer mechanism[33] but a continuous nucleation of nanoparticles so that all stages of species in the formation mechanism of fiber bundles can be more or less be observed simultaneously.[19] This is a result of the delayed release of Ba^{2+} from the polyacrylate complex.

Finally, a third stage in the time-resolved measurements is reached (zone III in Figure 5). This stage characterizes a situation close to equilibration as deduced from the constant pH and supersaturation in Figure 5. From the kinetics curves in Figure 5, it can be deduced that particle nucleation is nearly finished after 900 min. Nevertheless, a few particles are generated during this period, but Figure 7d clearly shows more particles than in the earlier images. Thus, it can be deduced that no particle growth occurs in the classical sense via lattice formation by ions, which would lead to a further decrease in supersaturation or a stop at $S = 1$. Instead, a mesoscale transformation of already-formed precursor nanoparticles is observed. Thus, it becomes understandable why structure development still proceeds, although the solution composition remains essentially unchanged. This finding nicely supports the results in our related study[19] that the fiber bundle formation takes place via the oriented attachment mechanism.[34−36] Here, high-energy surfaces are eliminated by crystallographic fusion to form defect-free linear single crystals or even aligned 3D bodies.[37−39]

From our related detailed mechanistic investigations, we reveal three different growth mechanisms for the fiber bundles, which will be discussed in detail elsewhere.[19] These mechanisms provide a full picture of the growth of $BaSO_4$ fibers in the presence of PAANa. However, one important finding from the consideration of the different growth mechanisms is that it is not clearly defined in the kinetic plots in Figure 5, at which time the different mechanism can be observed. Instead, different crystallization pathways appear to be simultaneously used depending on the locally available number of precursor nanoparticles.

Conclusions

This study has shown that the application of simple physical chemistry for solutions can yield remarkable insight into a complex additive-controlled mineralization process. By applying these methods to the polyacrylate-mediated morphogenesis of $BaSO_4$ fiber bundles composed of single-crystalline and defect-free $BaSO_4$ fibers,[10−16,19] we gain the following insights from the performed in situ measurements:

(a) A simple pH or conductivity titration can be used to determine interesting concentration regions for subsequent crystallization experiments for the precipitation of complex $BaSO_4$ fiber structures mediated by PAANa. It can be applied to any type of crystallization additive as long as the crystallization reaction or the reaction between the additive and ions or the crystal is pH-dependent.

(b) AUC, conductivity, and pH measurements as well as related supersaturation calculations reveal that Ba^{2+} is strongly complexed by PAANa, even after the addition of SO_4^{2-}. Low $BaSO_4$ supersaturation can be maintained by PAANa during the entire crystallization period. This complex inhibits the nucleation of $BaSO_4$, serves as precursor for crystallization, and shifts the crystallization mechanism from classical lattice formation from ions to the mesoscale assembly or transformation of precursor particles.[5] This is also evidenced by the observation that $BaSO_4$ fiber bundle formation does not correlate with time-dependent supersaturation.

(c) The final complex fibers are formed at a low supersaturation, as shown by optical microscopy. Mesoscale transformation

(33) LaMer, V. K.; Dinegar, R. H. *J. Am. Chem. Soc.* **1950**, *72*, 4847−4854.

processes,[5] which are particle-based, are generally different from classical ion-mediated crystallization, which is characterized by supersaturation. A combination of quantitative solution-based analysis (e.g., pH or conductivity) with techniques that are able to detect particles can determine whether a morphogenesis event takes place via the classical crystallization mechanism via lattice formation from ions or by mesoscopic alignment from preformed precursor particles.[5] This will be of interest especially for biomineralization examples, where many of their formation processes are still unknown, although amorphous nanoparticles often appear to play the role of precursor particles in the construction of more delicate mineral structures (e.g., calcium carbonate[40−45] or phosphate[46−51]).

Our results show that in addition to the particles, which are traditionally observed by microscopy, the first growth species can be accessed directly in solution by simple pH or conductivity measurements and that suitable additive-controlled crystallization conditions can be screened in an easy fashion. In addition, kinetic information on the complex mechanisms can be obtained by the correlation of microscopic images and kinetic information derived from time-dependent measurements. This is a very valuable tool for the characterization of complex growth mechanisms in additive-controlled mineralization, which are usually characterized by hierarchical structure over several orders of magnitude in size. In addition, the performed pH and conductivity measurements, supplemented by optical microscopy, are easy and cheap techniques and are available in almost every laboratory to characterize the species in solution. This can possibly help to solve some of the complex problems associated with the analysis of biomineralization and additive-controlled crystallization reactions, which are traditionally considered from the microscopic analysis viewpoint with the associated problems.

Acknowledgment. The Max Planck Society is gratefully acknowledged for financial support and a fellowship for T.W. We also thank Antje Völkel for AUC, Antje Reinecke for help with light microscopy, Dr. Charl Faul for time-dependent pH measurements, and Steffen Konzempel for conductivity measurements.

Appendix: Calculation of Time-Dependent Supersaturation

1. Relevant Reactions and Equilibrium Constants. There are four typical relevant reactions involved in $BaSO_4$ fiber generation: (1) acid dissociation and the equilibrium between PAA and PAANa with the acid-dissociation equilibrium constant K_a; (2) the complexation reaction between Ba^{2+} and the carboxylate groups of PAANa with the complexation constant K_c; (3) precipitation equilibrium with the solubility product of $BaSO_4$ K_{sp}; and (4) autodissociation of water with the dissociation constant K_w:

$$RCOOH + H_2O \overset{K_a}{\rightleftharpoons} RCOO^- + H_3O^+ \quad (1)$$

$$2RCOO^- + Ba^{2+} \overset{K_c}{\rightleftharpoons} (RCOO)_2Ba \quad (2)$$

$$BaSO_4 \overset{K_{sp}}{\rightleftharpoons} SO_4^{2-} + Ba^{2+} \quad (3)$$

$$H_2O + H_2O \overset{K_w}{\rightleftharpoons} H_3O^+ + OH^- \quad (4)$$

$$K_a = \frac{[RCOO^-][H_3O^+]}{[RCOOH]} \qquad K_c = \frac{[(RCOO)_2Ba]}{[Ba^{2+}][RCOO^-]^2}$$

$$K_{sp} = [SO_4^{2-}][Ba^{2+}] \qquad K_w = [H_3O^+][OH^-]$$

Note that all of the arrows in the above reactions are the forward/backward arrows, indicating that the reactions do not proceed completely to the right or left and all species coexisting in the equilibrium despite the comparably complete precipitate of $BaSO_4$ and the rather weak dissociation of water.

2. Composition of PAANa. The number-average molecular weight of PAANa is $M_n = 5100$ g/mol and the Na content is 19.0 wt %. This information was supplied by Fluka.

Additional analytical data consists of the following. Elemental analysis: C % = 34.34; H % = 5.10. Resulting molar ratios: C/Na = (C%/M_C)/(Na%/M_{Na}) = (34.34%/12.011)/(19.0%/22.990) = 2.86/0.83, where M_C and M_{Na} are the relative atomic masses of carbon and sodium. Measured water content: H_2O %(w/w) = 12.4%; therefore, the content of PAANa is PAANa % (w/w) = 87.6%.

3. Theoretical Concentration of Various Species in the Original Solution before the Addition of Ba^{2+} and SO_4^{2-}. *(a) Theoretical Concentration of Species in the Original Polymer Solution: $[RCOO^-]_{theo}$ and $[RCOOH]_{theo}$.* The solution of PAANa used for crystallization is [PAANa] = 561 mg/L

Because of the molar mass of PAANa of 5100 mg/mmol and the water content (12.4%) in the PAANa sample, the solution concentration is

$$[PAANa] = (561\ mg/L)\frac{1-12.4\%}{5100\ mg/mmol} = 9.63 \times 10^{-2}\ mmol/L$$

The structure of PAANa is

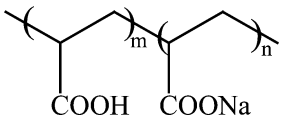

Its formula is $(C_3H_3O_2)_{m+n}H_mNa_n$. The unit number in the polymer chain is $m + n$.

As obtained above, the molar ratio of C to Na is 2.86/0.83, so C/Na = $3(m + n)/n$ = 2.86/0.83. Therefore, the percentage of carboxylic acid groups in the polymer is COOH% = $m/(m + n)$ = 12.9%.

(34) Penn R. L.; Banfield, J. F. *Geochim. Cosmochim. Acta* **1999**, *63*, 1549−1557
(35) Tang, Z. Y.; Kotov, N. A.; Giersig, M. *Science* **2002**, *297*, 237−240.
(36) Polleux, J.; Pinna, N.; Antonietti, M.; Niederberger, M. *Adv. Mater.* **2004**, *16*, 436−439
(37) Gehrke, N.; Cölfen H.; Pinna, N.; Antonietti, M.; Nassif, N. *Cryst. Growth Des.* **2005**, *5*, 1317−1319.
(38) Yang, H. G.; Zeng, H. C. *Angew. Chem.* **2004**, *116*, 6056−6059.
(39) Xu, A. W.; Antonietti, M.; Cölfen, H.; Fang, Y. P. *Adv. Funct. Mater.* **2006**, *16*, 903−908.
(40) Politi, Y.; Arad, T.; Klein, E.; Weiner, S.; Addadi, L. *Science* **2004**, *306*, 1161−1164.
(41) Raz, S.; Hamilton, P. C.; Wilt, F. H.; Weiner, S.; Addadi, L. *Adv. Funct. Mater.* **2003**, *13*, 480−486.
(42) Brecevil, L. *J. Cryst. Growth* **1989**, *98*, 504.
(43) Addadi, L.; Raz, S.; Weiner, S. *Adv. Mater.* **2003**, *15*, 959−970.
(44) Loste, E.; Meldrum, F. C. *Chem. Commun.* **2001**, *10*, 901−902.
(45) Xu, X.; Han, J. T.; Kim, D. H.; Cho, K. *J. Phys. Chem. B* **2006**, *110*, 2764−2770
(46) Sinyaev, V. A.; Shustikova, E. S.; Levchenko, L. V.; Sedunov, A. A. *Inorg. Mater.* **2001**, *37*, 619−622.
(47) Yin, X. L.; Stott, M. J. *J. Chem. Phys.* **2003**, *118*, 3717−3723
(48) Somrani, S.; Rey, C.; Jemal, M. *J. Mater. Chem.* **2003**, *13*, 888−892.
(49) Rodrigues, A.; Lebugle, A. *J. Solid State Chem.* **1999**, *148*, 308−315
(50) Posner, A. S.; Betts, F. *Acc. Chem. Res.* **1975**, *8*, 273−281
(51) Betts, F.; Blumenthal, N. C.; Posner, A. S.; Becker, G. L.; Lehninger, A. L. *Proc. Nat. Acad. Sci. U.S.A.* **1975**, *72*, 2088−2090.

To simplify the calculation, assume PAANa to be a solution of a monoprotic acid instead of a polyprotic acid:

On the basis of elemental analysis data of C% = 34.34, and Na% = 19.0, the concentration of the initial species in the PAANa solution is

$$\text{total concentration of carbon atoms} = [\text{C}]_{\text{total}} = 561\ \text{mg/L} \times \text{C\%}/M_{\text{C}} = 561\ \text{mg/L} \times 34.34\%/12.011\ \text{mg/mmol} = 16.05\ \text{mmol/L}$$

Because there are three carbon atoms in each unit of PAANa, the total carboxylate concentration is

$$[\text{RCOO}^-]_{\text{total}} = \frac{16.05\ \text{mmol/L}}{3} = 5.35\ \text{mmol/L}$$

The concentrations of the salt form of carboxylate and sodium is

$$[\text{RCOO}^-]_{\text{theo}} = [\text{Na}^+] = (561\ \text{mg/L})\frac{\text{Na\%}}{22.98977} = (561)\frac{19.0\%}{22.98977} = 4.63\ \text{mmol/L}$$

Therefore, the theoretical concentration of the acid form is $[\text{RCOOH}]_{\text{theo}} = 5.35\ \text{mmol/L} - 4.63\ \text{mmol/L} = 0.72\ \text{mmol/L}$.

In summary, the theoretical concentrations of the different species in PAANa solution are $[\text{PAANa}] = 9.63 \times 10^{-2}$ mmol/L, $[\text{RCOO}^-]_{\text{total}} = 5.35$ mmol/L, $[\text{RCOO}^-]_{\text{theo}} = 4.63$ mmol/L, and $[\text{RCOOH}]_{\text{theo}} = 0.72$ mmol/L.

(b) Equilibrium Concentration of Different Species in PAANa: $[RCOOH]_{equilibrium}$ and $[RCOO^-]_{equilibrium}$. Because the degree of dissociation of PAA or the degree of protonation of PAA^- is weak, the dissociation of water must be considered when the solution pH is calculated (eq 4). The experimentally measured pH of the solution is 8.4 when the concentrion of PAANa is 561 mg/L. Therefore, the total concentration of protons is $[\text{H}^+] = 10^{-8.4}$ mol/L. On the basis of the ion product constant of water ($K_w = 10^{-14}\ \text{mol}^2/\text{L}^2$) at room temperature, the total concentration of hydroxide ions in such PAANa solution is $[\text{OH}^-] = 10^{-5.6}$ mol/L, respectively, shown as equilibrium in eq 5.

In the PAANa solution, the total number of H^+ ions can be dissociated from H_2O and PAA acid, but the total number of OH^- ions can be generated only by the dissociation of H_2O. Because $[\text{OH}^-] > [\text{H}^+]$, the totally dissociated H_2O is actual $10^{-5.6}$ mol/L, shown as dissociation in eq 5, and part of the protons are consumed by the protonation of PAANa, shown as consumed by PAA^- in eq 5, which leads to a basic solution.

$$\underset{\text{equilibrium (mol/L):}}{\text{H}_2\text{O}} + \underset{\text{variation (mol/L):}}{\text{H}_2\text{O}} \underset{}{\overset{K_w}{\rightleftharpoons}} \underset{\text{consumed by PAA}^- \text{ (mol/L):}}{\text{H}_3\text{O}^+} + \text{OH}^- \quad (5)$$

	H_2O	H_2O	H_3O^+	OH^-
equilibrium (mol/L):			$10^{-8.4}$	$10^{-5.6}$
variation (mol/L):	$-10^{-5.6}$	$-10^{-5.6}$	$+10^{-5.6}$	$+10^{-5.6}$
consumed by PAA^- (mol/L):			$10^{-5.6}-10^{-8.4}$	

In fact, the measured basic solution (pH 8.4) means that the protonation of carboxylate ($-\text{COO}^-$) is higher than the dissociation of PAA ($-\text{COOH}$) in the system.

Furthermore, the proton consumption by PAA^- through the protonation of PAA^- into PAA can be shown as the reverse reaction of eq 6 and "variation". Here, "initial" means the theoretical concentration when PAANa was regarded as not being further dissociated or protonated. The equilibrium is the actual concentration of carboxylic acid or carboxylate ions, which can be calculated as follows in eq 6.

$$\underset{\text{initial (mmol/L):}}{\text{RCOOH}} + \text{H}_2\text{O} \underset{}{\overset{K_a}{\rightleftharpoons}} \underset{\text{variation (mol/L):}}{\text{H}_3\text{O}^+} + \underset{\text{equilibrium (mmol/L):}}{\text{RCOO}^-} \quad (6)$$

	RCOOH	H_3O^+	$RCOO^-$
initial (mmol/L):	0.72		4.63
variation (mol/L):	$+(10^{-5.6}-10^{-8.4})$	$-(10^{-5.6}-10^{-8.4})$	$-(10^{-5.6}-10^{-8.4})$
equilibrium (mmol/L):	$0.72 + (10^{-5.6}-10^{-8.4}) \times 10^3$		$4.63 - (10^{-5.6}-10^{-8.4}) \times 10^3$

In summary, the concentrations of the different species in the equilibrium PAANa solution are $[\text{H}^+]_{\text{equilibrium}} = 10^{-8.4}$ mol/L, $[\text{OH}^-]_{\text{equilibrium}} = 10^{-5.6}$ mol/L, $[\text{RCOOH}]_{\text{equilibrium}} = 0.72\ \text{mmol/L} + 10^3(10^{-5.6}-10^{-8.4})\ \text{mmol/L} \cong 0.72$ mmol/L, and $[\text{RCOO}^-]_{\text{equilibrium}} = 4.63\ \text{mmol/L} - 10^3(10^{-5.6}-10^{-8.4})\ \text{mmol/L} \cong 4.63$ mmol/L.

Therefore, the observed equilibrium constant of PAANa can be obtained by the following equation when PAANa is taken as a monoprotonic acid

$$K_a = \frac{[\text{RCOO}^-][\text{H}_3\text{O}^+]}{[\text{RCOOH}]}$$

$$K_a(\text{observed}) = (4.63\ \text{mmol/L} \times 10^{-3})\frac{10^{-8.4}\ \text{mol/L}}{0.72\ \text{mmol/L} \times 10^{-3}} = 2.6 \times 10^{-8}\ (\text{mol/L})$$

Note that although the average pK_a value for PAA from the literature is in the range of 5.8−6.4,[52] which is considerably lower than our observed constant, we consider our observed equilibrium constant to be reasonable in this system. The difference is possible from the only assumption that poly(acrylic acid) is a monoprotic acid, which is usually used in analytical chemistry for simplification of pH calculations.

4. Molar Ratios, *R*, of Ba^{2+} and $RCOO^-$ from PAANa with the Addition of $BaCl_2$ to PAANa ($R = [Ba^{2+}]_{total}/[RCOO^-]_{total}$). In the titration of Ba^{2+} into PAANA solution, defined volumes of $BaCl_2$ (50 mol/L) were added to 15 mL of PAANa (0.56 g/L) solution.

From the above calculation in step 3, the total concentration of carboxylate and carboxylic acid, $[\text{RCOO}^-]_{\text{total}}$, in PAANa is $[\text{RCOO}^-]_{\text{total}} = 5.35$ mmol/L.

If the added volume of Ba^{2+} is V_{added} (mL), then the concentration of Ba^{2+} can be defined as

$$[\text{Ba}^{2+}]_{\text{added}} = \frac{50\ \text{mmol/L} \times V_{\text{added}}}{15\ \text{mL} + V_{\text{added}}}$$

If the addition volume is known, then the molar ratio, *R*, can be directly calculated from

$$R = \frac{[\text{Ba}^{2+}]_{\text{total}}}{[\text{RCOO}^-]_{\text{total}}} = \frac{(50\ \text{mmol/L} \times V_{\text{added}})/(15\ \text{mL} + V_{\text{added}})}{5.35\ \text{mmol/L}}$$

For example, when the volume additions are 0.6, 0.65, and 0.8 mL, the molar ratio *R* can be obtained as 0.375 (point A in Figure 2), 0.4, and 0.5 (point B in Figure 2), respectively.

(52) Zhien-Chi, C.; Ring, T. A.; Lemaitre, J. *J. Am. Ceram. Soc.* **1992**, *75*, 3201−3208.

5. Time-Dependent Concentration of Different Species during Crystallization after the Addition of Ba^{2+} and SO_4^{2-}. *(a) Practical Concentration of RCOOH and $RCOO^-$ after the Addition of Ba^{2+} and SO_4^{2-}: $[RCOOH]_{original}$ and $[RCOO^-]_{original}$.* When Ba^{2+} is added to PAANa solution, the solution pH changes from 8.4 to 5.7, which implies that some RCOOH is dissociated into protons and $RCOO^-$. The practical concentration of RCOOH is obtained according to eq 1:

$$[\mathrm{RCOOH}]_{\mathrm{original}} = [\mathrm{RCOOH}]_{\mathrm{theo}} - [\mathrm{RCOOH}]_{\mathrm{dissociated}} = 0.72\ \mathrm{mmol/L} + (10^{-\mathrm{pOH}} - 10^{-\mathrm{pH}})10^{-3}\ \mathrm{mmol/L} \cong 0.72\ \mathrm{mmol/L}$$

However, because of the formation of the $(RCOO)_2Ba$ complex between Ba^{2+} and $[RCOO^-]$ shown as eq 2, the concentration of $RCOO^-$ will decrease with the addition of Ba^{2+}, and the practical concentration of $RCOO^-$ cannot be taken as the theoretical concentration as for RCOOH.

(b) Time-Dependent pH: $[H^+]_{time}$. This was taken directly from time-dependent pH measurements.

(c) Time-Dependent Practical Concentration of RCOOH in the Crystallization Solution: $[RCOOH]_{time}$. During crystallization, the total $[RCOOH]_{time}$ is composed of the original RCOOH, $[RCOOH]_{original}$, and that from the protonated $[RCOO^-]$, which is released from the complex of $(RCOO)_2Ba$ (eq 2). Therefore, $[RCOOH]_{time} = [RCOOH]_{original} + [RCOO^-]_{protonated}$.

The increasing of [RCOOH] is closely related to the decreasing proton concentration according to eq 1. As a matter of fact, the variation of the time-dependent pH over the whole mineralization regime is small (e.g. pH from 5.7 to 7.2). Therefore, $[RCOOH]_{time} = 0.72\ \mathrm{mmol/L} + (10^{-\mathrm{pOH}} - 10^{-\mathrm{pH}})\ \mathrm{mol/L} \cong 0.72\ \mathrm{mmol/L}$.

The practical concentration of RCOOH in solution, $[RCOOH]_{time}$, has no large effect on the base in eq 6 and can be taken as a constant with its initial concentration.

(d) Time-Dependent Practical Concentration of $RCOO^-$ in Solution: $[RCOO^-]_{time.}$ In comparison to no detectable change of the $[RCOOH]_{time}$, the time-dependent concentration of $RCOO^-$, $[RCOO^-]_{time}$, will change because of the dissociation of the $(RCOO)_2Ba$ complex (eq 2). However, $[RCOO^-]_{time}$ will be also restrained by eq 1

Therefore, after $[H^+]$ is obtained directly from a time-dependent pH measurement, $[RCOO^-]_{time}$ can be calculated from eq 1

$$[\mathrm{RCOO^-}]_{\mathrm{time}} = \frac{K_a[\mathrm{RCOOH}]_{\mathrm{time}}}{[\mathrm{H^+}]_{\mathrm{time}}}$$

where $K_a = 2.6 \times 10^{-8}$ (mol/L) and $[RCOOH]_{time} \cong 0.72$ mmol/L.

During crystallization, we define the variation in $RCOO^-$ concentration as $\Delta[RCOO^-]$, which refers to those ions released from the $(RCOO)_2Ba$ complex (shown in eq 2)

$$\Delta[\mathrm{RCOO^-}] = [\mathrm{RCOO^-}]_{\mathrm{time}} - [\mathrm{RCOO^-}]_{\mathrm{original}}$$

where $[RCOO^-]_{original}$ is the practical concentration of $RCOO^-$ at the beginning of mineralization after the addition of Ba^{2+} and SO_4^{2-} ions to the PAANa solution.

Then, the time-dependent concentration of $[Ba^{2+}]$ released from the complex can be shown as

$$[\mathrm{Ba^{2+}}]_{\mathrm{released}} = \frac{1}{2}[\Delta[\mathrm{RCOO^-}] = \frac{1}{2}([\mathrm{RCOO^-}]_{\mathrm{time}} - [\mathrm{RCOO^-}]_{\mathrm{original}})$$

(e) Time-Dependent Concentration of the Complex: $[(RCOO)_2Ba]_{time}$. The typical solution for mineralization is prepared by the addition of 0.6 mL of 0.05 mol·L^{-1} $BaCl_2$ and 0.6 mL of 0.05 mol·L^{-1} Na_2SO_4 to 15 mL of PAANa (0.56 g·L^{-1}) in a glass bottle under vigorous stirring. Therefore, the total concentration of $[Ba^{2+}]_0 = [SO_4^{2-}]_0$ should be

$$\frac{0.6\ \mathrm{mL} \times 0.05\ \mathrm{mol/L}}{(15 + 0.6 + 0.6)\ \mathrm{mL}} = 1.85\ \mathrm{mmol/L}$$

The total concentration of $[Ba^{2+}]$ in solution is 1.85 mmol/L, and $[RCOO^-]_{total}$ in solution is 5.35 mmol/L. It is reasonable to assume that most of the Ba^{2+} ions are complexed by $RCOO^-$. In fact, pH measurements and conductivity titration of PAANa upon addition of Ba^{2+} as well as AUC show that Ba^{2+} is almost completely complexed by PAANa (Figures 1−3). Therefore, the concentration of the complex in the original solution, $[(RCOO)_2Ba]_0$, can be approximately taken as the same value as the original Ba^{2+} concentration, $[Ba^{2+}]_0$:

$$[(\mathrm{RCOO})_2\mathrm{Ba}]_0 = [\mathrm{Ba^{2+}}]_0 = [\mathrm{SO_4^{2-}}]_0 = 1.85\ \mathrm{mmol/L}$$

Then, the time-dependent concentration of the complex in solution can be calculated as

$$[(\mathrm{RCOO})_2\mathrm{Ba}]_{\mathrm{time}} = [(\mathrm{RCOO})_2\mathrm{Ba}]_0 - [\mathrm{Ba^{2+}}]_{\mathrm{released}} = [\mathrm{Ba^{2+}}]_0 - [\mathrm{Ba^{2+}}]_{\mathrm{released}} = [\mathrm{Ba^{2+}}]_0 - \frac{1}{2}\Delta[\mathrm{RCOO^-}]$$

where $\Delta\{[RCOO^-]\}$ is $[RCOO^-]$ released from the complex.

(f) Time-Dependent Real Concentration of Ba^{2+} in Solution: $[Ba^{2+}]_{time.}$ In eq 2,

$$K_c = \frac{[(\mathrm{RCOO})_2\mathrm{Ba}]}{[\mathrm{RCOO^-}]^2\,[\mathrm{Ba^{2+}}]}$$

Therefore,

$$[\mathrm{Ba^{2+}}]_{\mathrm{time}} = \frac{[(\mathrm{RCOO})_2\mathrm{Ba}]_{\mathrm{time}}}{[\mathrm{RCOO^-}]_{\mathrm{time}}^2 K_c}$$

where $[(RCOO)_2Ba]_{time}$ and $[RCOO^-]_{time}$ are the time-dependent concentrations of the $(RCOO)_2Ba$ complex and $RCOO^-$ ion and can be calculated as shown above in steps d and e. Nevertheless, K_c is still an unknown constant.

(g) Time-Dependent Practical Concentration of SO_4^{2-} in Solution: $[SO_4^{2-}]_{time}$. $[SO_4^{2-}]_{time} = [SO_4^{2-}]_0 - [BaSO_4]_{time}$, in which $[SO_4^{2-}]_0$ is the original concentration of SO_4^{2-} at the beginning of mineralization.

We define $[BaSO_4]$ as the molar amount of $BaSO_4$ crystals per liter. Therefore,

$$[\mathrm{BaSO_4}]_{\mathrm{time}} = [\mathrm{Ba^{2+}}]_{\mathrm{released}} - [\mathrm{Ba^{2+}}]_{\mathrm{time}}$$

Then,

$$[\mathrm{SO_4^{2-}}]_{\mathrm{time}} = [\mathrm{SO_4^{2-}}]_0 - [\mathrm{BaSO_4}]_{\mathrm{time}} = [\mathrm{SO_4^{2-}}]_0 - \{[\mathrm{Ba^{2+}}]_{\mathrm{released}} - [\mathrm{Ba^{2+}}]_{\mathrm{time}}\}$$

6. Time-Dependent Supersaturation. If the concentration can be used instead of activity, then supersaturation can be defined as

$$S = \left\{ \frac{[SO_4^{2-}]_{time}\,[Ba^{2+}]_{time}}{K_{sp}} \right\}^{0.5}$$

where $K_{sp} = 1.07 \times 10^{-10}$ (mol^2/L^2). A combination of all of the above calculations yields

(1) $[SO_4^{2-}]_{time} = [SO_4^{2-}]_0 - \{[Ba^{2+}]_{released} - [Ba^{2+}]_{time}\}$, $[SO_4^{2-}]_0 = 1.85$ mmol/L;

(2) $[Ba^{2+}]_{time} = [(RCOO)_2Ba]_{time}/[RCOO^-]_{time}^2 K_c$, where $[(RCOO)_2Ba]_{time} = [Ba^{2+}]_0 - [Ba^{2+}]_{released}$ and $[Ba^{2+}]_0 = 1.92$ mmol/L. $[RCOO^-]_{time} = K_a[RCOOH]_{time}/[H^+]_{time}$, in which $K_a = 2.6 \times 10^{-8}$ (mol/L) and $[RCOOH]_{time} \cong 0.72$ mmol/L. K_c is unknown.

(3) $[Ba^{2+}]_{released} = {}^1/_2[\Delta[RCOO^-] = {}^1/_2\,([RCOO^-]_{time} - [RCOO^-]_{original})$, $[RCOO^-]_{original} = K_a\,[RCOOH]_{original}/[H^+]_{original}$, $[RCOOH]_{original} \cong 0.72$ mmol/L, and $[H^+]_{original} = 10^{-5.7}$ mol/L.

Therefore, because $[H^+]_{time}$ can be measured directly, the only unknown parameters are K_c and S.

To calculate the time-dependent supersaturation, we make the reasonable assumption that the supersaturation is $S = 1$ at the end of mineralization:

$$S_{end} = \left\{ \frac{[SO_4^{2-}]_{time}\,[Ba^{2+}]_{time}}{K_{sp}} \right\}^{0.5} = 1$$

$$[SO_4^{2-}]_{time} = [SO_4^{2-}]_0 - \{[Ba^{2+}]_{released} - [Ba^{2+}]_{time}\}$$

$$[SO_4^{2-}]_0 = 1.85\ \text{mmol/L} = 1.85 \times 10^{-3}\ \text{mol/L}$$

The final released concentration of Ba^{2+} can be calculate as described above:

$$[Ba^{2+}]_{released} = 7.18 \times 10^{-6}\ \text{mol/L}$$

The time-dependent concentration of Ba^{2+} is

$$[Ba^{2+}]_{time} = \frac{[(RCOO)_2Ba]_{time}}{[RCOO^-]_{time}^2 K_c}$$

The concentrations of both $[(RCOO)_2Ba]_{time}$ and $[RCOO^-]_{time}$ can be calculated as above. Therefore,

$$[Ba^{2+}]_{time} = \frac{[(RCOO)_2Ba]_{time}}{[RCOO^-]_{time}^2 K_c} = \frac{3.144 \times 10^6}{K_c}$$

From $\{[SO_4^{2-}]_{time}\,[Ba^{2+}]_{time}/K_{sp}\}^{0.5} = 1$, we find that

$$\left\{1.85 \times 10^{-3} - \left(7.18 \times 10^{-6} - \frac{3.144 \times 10^6}{K_c}\right)\right\} \times \left(\frac{3.144 \times 10^6}{K_c}\right) = 1.07 \times 10^{-10}$$

Then, K_c can be obtained as $K_c = 5.44 \times 10^{13}$ (mol/L)$^{-2}$.

From a combination of all of the parameters obtained from step 6 and by introducing K_c into time-dependent $[SO_4^{2-}]_{time}$ and $[Ba^{2+}]_{time}$, the time-dependent supersaturation can be obtained.

Supporting Information Available: Full video sequence of time-dependent optical microscopy from the same observed area at different crystallization times. This material is available free of charge via the Internet at http://pubs.acs.org.

LA0609827